UNIVERSITIY OF CALIFORNIA SAN DIEGO

Nonstructural Protein 4 Alone of the Severe Acute Respiratory Syndrome Coronavirus-2 (SARS-CoV-2) Causes Significant Alterations of Host Endoplasmic Reticulum (ER) Structure and Inheritance in *S. cerevisiae*.

A thesis submitted in partial satisfaction of the requirements
for the degree of Master of Science

in

Biology

by

Allison Kifer

Committee in charge:

Professor Maho Niwa, Chair
Professor Andreas Ernst
Professor James Kadonaga

2022

The Thesis of Allison Kifer is approved, and it is acceptable in quality and form for publication on microfilm and electronically.

University of California San Diego

2022

DEDICATIONS

I dedicate this Thesis to my parents, who taught me how to face and overcome adversity with grace, and to my community of mentors, friends, and peers. Thank you for your endless support.

TABLE OF CONTENTS

LIST OF ABBREVIATIONS

SARS-CoV-2	Severe acute respiratory syndrome coronavirus 2
MERS	Middle eastern respiratory syndrome
CoV	Coronavirus
DMV	Double-membrane vesicle
+RNA	Positive strand RNA
ER	Endoplasmic reticulum
Nsp4	Nonstructural protein 4
ERSU	ER Stress Surveillance pathway
UPR	Unfolded protein response
ESCRT	Endosomal sorting complex required for transport
ERGIC	ER-Golgi intermediate compartment
COP	Coat Protein Complex
ERAD	ER-associated degradation
Vps	Vacuolar protein sorting
Pho88	Phosphate transfer protein 88
GFP	Green fluorescent protein
cER	Cortical ER
pnER	Perinuclear ER
MAP	Mitogen activated protein
Ire1	Inositol requiring enzyme 1
Gal	Galactose

Raff	Raffinose
CRM	Cytokinetic remnant
Tm	Tunicamycin
MVB	Multivesicular body
HMG-CoA	3-hydroxy-3-methylglutaryl coenzyme A
CW	Calcofluor white
DIC	Differential image contrast
DAPI	4’,6-diamidino-2-phenylindole

LIST OF FIGURES

LIST OF TABLES

ACKNOWLEDGMENTS

First and foremost, I would like to acknowledge and express my gratitude to Dr. Maho Niwa for her guidance and support as chair of my committee. It was through Dr. Niwa's expertise and mentorship that my growth as a researcher and the culmination of this Thesis was made possible. Dr. Niwa taught me how to be curious, both as an academic and as an individual, and I will be forever grateful.

I would also like to acknowledge Dr. Andreas Ernst and Dr. James Kadonaga for joining and supporting my thesis committee. They have both inspired confidence in me throughout my time in the BS/MS program, inside and outside of the classroom, and I am immensely grateful for their advice and encouragement.

Finally, I would like to acknowledge the members of the Niwa lab, who have worked through setbacks with me, mentored me, and have made me, in turn, a better mentor. I cannot express how thankful I am for the trust, companionship, and kindness I have received from my time in the Niwa lab.

ABSTRACT OF THE THESIS

Nonstructural Protein 4 Alone of the Severe Acute Respiratory Syndrome Coronavirus-2 (SARS-CoV-2) Causes Significant Alterations of Host Endoplasmic Reticulum (ER) Structure and Inheritance in *S. cerevisiae*.

by

Allison Kifer

Master of Science in Biology

University of California San Diego, 2022

Professor Maho Niwa, Chair

When the novel coronavirus SARS-CoV-2 infects human cells, it results in the formation of "double-membrane vesicles" (DMVs) upon major rearrangements of the host cell compartment called the endoplasmic reticulum (ER) (Cortese *et al.*, 2020). Previous studies have identified that nonstructural protein 4 (Nsp4), one of SARS-CoV-2 coded proteins, is involved in formation of the DMVs in mammalian cells (Angelini *et al.*, 2013; Hagemeijer *et al.*, 2014; Oudshoorn *et al.*, 2017). Importantly without proper DMV formation, SARS-CoV are unable to replicate and reproduce in the infected cell (Sakai *et al.*, 2017). Little is known about if host cell components are

involved and the molecular mechanisms by which the DMV is formed. In order to answer these questions, we used a minimal experimental model and transformed a plasmid that expresses SARS-CoV-2 Nsp4 under the galactose regulatable promoter into wild type *Saccharomyces cerevisiae,* or budding yeast. These cells carried a prominent ER transmembrane protein fused with GFP (Pho88-GFP) integrated in the genomic *pho88* locus. Here, we show that expression of Nsp4 alone in WT cells results in the dramatic rearrangement of ER structure. Using gene knockout cell strains, we found that while upstream elements of ER stress mitigating pathways like the unfolded protein response (UPR) and ER stress surveillance (ERSU) checkpoint were not involved in these rearrangements, proteins Vps4 and Vps24 of the endosomal sorting complexes required for transport (ESCRT) were involved. Finally, we discovered that inducing Nsp4 expression results in a significant decrease of ER inheritance into the daughter cell and is mediated in part by Vps4. This minimal experimental approach allows for a further investigation of host components involved in both morphological and functional changes of the ER and potential drug targets to disrupt DMVs, and thus SARS-CoV-2 reproduction.

INTRODUCTION

Coronaviruses (CoVs) in the subfamily *Coronavirinae* are enveloped positive strand RNA (+RNA) viruses that are transmissible to vertebrates, including humans, and cause health concerns of varying effects (Hartenian *et al.,* 2020). Novel CoVs, including severe acute respiratory syndrome coronavirus 2 (SARS-CoV-2), SARS-CoV, and the Middle East respiratory syndrome (MERS)-CoV all belong to the betacoronavirus family and are responsible for human outbreaks in 2019, 2003, and 2012, respectfully. The CoV genome is extremely large compared to other +RNA viruses, between 26-33 kbp in length, and encodes for structural, accessory and nonstructural proteins (Nsps) (Gordon *et al.,* 2020). Upon entry into host cells, the +RNA genome can be immediately translated, in contrast to DNA viruses, to generate two polyproteins. These polyproteins are further processed to produce the array of viral proteins in the cytoplasm, specifically translated on the surface of the host endoplasmic reticulum (ER) (Gordon *et al.,* 2020). Nsp1-16 are all important for differing stages of the viral life cycle and translocate based on their viral function, with some entering into the ER, moving to the ER-Golgi intermediate compartment (ERGIC), and finally the cis-golgi, where assembly of the CoV occurs (Klumperman *et al.,* 1994; Sicari *et al.,* 2020).

In addition to translation, +RNA genome replication for MERS-CoV and SARS-CoV occurs upon the modification of the ER into elaborate vesicle-like structures called double-membrane vesicles (DMVs) (Angelini *et al.,* 2013; Knoops *et al.,* 2008; Oudshoorn *et al.,* 2017). In fact, recent studies revealed that infection of SARS-CoV-2 generates similar DMV structures with some CoV-2 specificities (Cortese *et al.,* 2020).

Associated with the DMV, host cell translation components such as ribosomes and transcription factors are found along with the +RNA genome (Snijder *et al.,* 2020; Wolff *et al.,* 2020). While functional roles of SARS-CoV-2 DMVs require further experiments, it has been proposed that formation of DMVs allow protection of the +RNA genome and concentration of the host gene translational components including polyribosomes (Miller and Krijnse-Locker, 2008; Shulla and Randall, 2016). The importance of understanding the mechanism of DMV formation is underscored by inhibition of viral replication, and thus reproduction, in its absence (Sakai *et al.,* 2017). These results suggest that understanding the host cell components and the molecular mechanisms of DMV formation may ultimately point to identification of effective drugs or methods that can block the DMV formation, thus limiting CoV reproduction and infection of the host.

Given the complex structure of DMVs and associated ER changes, understanding how DMVs are formed from the host ER membrane in a simplified model system will hold a promise towards functional significance of DMVs. An interesting feature of the betacoronavirus family is that the expression of just one of three ER localized Nsp genes in either mammalian tissue culture or yeast cells can cause changes in ER morphology. For example, co-transfection of Nsp3, Nsp4, and Nsp6 from the severe acute respiratory syndrome (SARS)-CoV in Human Embryonic Kidney (HEK)283T cells were sufficient to generate DMV-like structure, referred as ER-associated replication organelles (Angelini *et al.*, 2013). Similar DMV structures were generated from host ER in cells infected with Nsp4 and Nsp3 from MERS-CoV (Oudshoorn *et al.*, 2017).

The ER is one of the major compartments in eukaryotic cells and plays critical functional roles including membrane and secretory protein maturation, lipid biosynthesis pathways and metabolism, the detoxification of unwanted chemicals, and the regulation of Ca2+ storage (Cohen, Valm, and Lippincott-Schwartz, 2018; Hurst and Fratti, 2020; Karagas and Venkatachalam, 2019). Only properly folded secretory proteins can be packaged into Coat Protein Complexes (COP) to leave the ER and reach the Golgi via transit through the ERGIC (Appenzeller-Herzog and Hauri, 2006). In addition to playing a variety of functions, the ER functional capacities must be adjusted in response to the cellular needs of environmental and developmental cues. This is achieved, in part, by a well-studied signal transduction pathway called the Unfolded Protein Response (UPR) to ensure both overall size, shapes and functional capacities of the ER meet the demands of the cell (Kozutsumi *et al.*,1988; Mori, 2000). Exceeding the functional capacity of the ER and its various functions, such as increasing protein production, lipid biosynthesis production, or depletion of calcium storage, are considered contributors of canonical "ER stress" (Fun and Thibault, 2020). The elevated demand to synthesize secretory proteins is mitigated by the UPR by upregulating the transcription of genes coding for ER protein folding and modifying components (Ron and Walter, 2007). Permanently misfolded proteins are detected by UPR factors that will then upregulate ER-associated degradation (ERAD) and rid the cell of unwanted proteins (Hampton and Sommer, 2012). Furthermore, the ER cannot be generated *de novo***,** and thus, the ER functions and overall ER levels and sizes may require to be properly regulated during the cell cycle (Niwa, 2020).

The ER in mammalian cells is continuous with the outer nuclear membrane and extends outward to form a reticular structure that is spread extensively throughout the cytoplasm (Schwarz and Blower, 2016). When compared to mammalian ER, yeast ER is much simpler structurally (Fehrenbacher *et al*., 2002). Perinuclear ER (pnER) is seen near or surrounding the nucleus, with connections to the nuclear envelope and peripheral or periplasmic ER, often referred to as cortical ER (cER), that is juxtaposed with the plasma membrane. Tubular ER connects between cER and pnER, and while most ER proteins are found in both types of ER, some proteins are more enriched in one type of the ER over the other (Preuss *et al.*, 1998). The ER is also a dynamic organelle and during the early stage of the cell cycle in yeast, the tubular ER emanated from the pnER points towards the incipient bud site, followed by its entry into the daughter cell (Chao, Piña, and Niwa, 2021). Ultimately, the tubular ER is anchored to the bud tip, or the furthest point of the daughter cell, by its interactions with bud tip localized proteins. Upon anchoring to the bud tip, the ER tubule changes the direction of its growth, spreading the tubular ER along the cortex of the daughter cell (Chao, Piña, and Niwa, 2021). While certain components are known to mediate the movement of the ER under the normal cell cycle, mechanisms of the ER morphological and structural changes remain elusive at this point.

Given the simpler structure of the ER and smaller yeast genome, yeast often serves as an ideal experimental system for varieties of cellular events (Botstein and Fink, 2011). Based on the previous studies discussed, expression and studying the consequences of one or more of the three SARS-CoV-2 ER-associated proteins will likely facilitate mechanistic and functional understanding of their impacts on overall ER

structure and functional homeostasis including the ER inheritance. Ultimately, those studies will allow molecular dissection of DMV formation of the SARS-CoV-2. Additionally, the budding yeast experimental model offers opportunities to dissect the effects of nonstructural protein expression on ER homeostasis including the host ER distributions within the cell and ER inheritance.

Previously, the Niwa lab identified that there exists an ER inheritance checkpoint independent of the UPR, which they termed as the ER Stress Surveillance (ERSU) pathway in budding yeast (Babour *et al.*, 2010). The ERSU pathway responds to ER stress by blocking the inheritance of "stressed cortical ER" into the daughter cell and translocates a complex known as the septin ring away from the bud neck, ultimately leading to cytokinesis halt (Babour *et al.*, 2010). If ER stress is mitigated and functional homeostasis is reestablished, the cytokinesis block is lifted, allowing cells to reenter the cell cycle and inherit functional ER (Babour *et al.*, 2010). Thus, the ERSU pathway works in tandem with yet independently of the UPR to ensure the inheritance of "stress free" ER that can keep up with functional demand.

The ERSU pathway is regulated by the mitogen activated protein (MAP) kinase Slt2, independent from the UPR regulatory transmembrane kinase Ire1 (Babour *et al.*, 2010). The ERSU pathway involves the septin ring, which is a dynamic complex that assembles at the incipient bud. The septin ring is thought to function as a diffusion barrier to aid in the complex process of intracellular inheritance into the daughter, although the exact mechanisms employed at the diffusion barrier are not well understood. In response to ER stress, mislocalization of the septin ring away from the bud neck to a location called the cytokinetic remnant (CRM) leads to cytokinesis halt

(Chao *et al.*, 2019). Thus, the ERSU pathway ensures that "stressed ER" will not enter the daughter. In *ire1Δ* cells, the septin ring is unable to translocate and "stressed cER" enters into the daughter, leading to the subsequent death of both the mother and daughter cells (Babour *et al.*, 2010).

In this thesis, we investigated the impact of SARS-CoV-2 Nsp4 and the potential effects of its expression on the ER functional homeostasis. In order to address these questions, we transformed a plasmid that expresses SARS-CoV-2 Nsp4 under the galactose regulatable promoter into wild type (WT) budding yeast cells. These cells carried a well-characterized ER transmembrane protein fused with GFP (Pho88-GFP) integrated in the genomic *pho88* locus. We then induced the expression of Nsp4 and observed the following effects on ER morphology via live light microscopy. Furthermore, establishment of this experimental system will allow testing of a subset of ER genes associated with various ER functions, such as UPR associated ERAD and ERSU elements, COPII or COPI vesicle components, and other genes that may allow for major changes of host membranes. Ultimately, it will allow an unbiased approach to screen and identify the genes involved without any prior knowledge. This led us to initiate searches of host proteins involved in the Nsp4-induced ER morphological changes. As a pilot, we tested the UPR and ERSU components, Ire1 and Slt2, respectively and proteins of the endosomal sorting complex required for transport (ESCRT), which are widely involved in various membrane altering processes, including cytokinesis and endocytic vesicle formations. Our results suggest that the expression of Nsp4 has distinct effects on ER functional structure, morphology, and inheritance,

thereby validating that the yeast experimental system described here can serve to set up a genome wide screen for identification of host proteins involved.

.

RESULTS

SARS-CoV-2 Nsp4 expression leads to significant changes in host ER membrane alteration

Based on the homologies to other members of the coronavirus family, three nonstructural proteins (Nsps), Nsp3, 4, and 6, are reported to play roles in the generation of double-membrane vesicles (DMVs) upon alterations of the ER membrane. To begin elucidating the roles of these viral Nsps in the formation of DMVs, we expressed SARS-CoV-2 Nsp4 under a regulatable promoter in WT BY4741 haploid yeast, *S. cerevisiae,* carrying a genomically integrated green fluorescent protein (GFP) tagged form of Pho88 (Pho88-GFP). In this reporter, the C-terminus of Pho88, an ER transmembrane protein, is fused to GFP, which allows visualization of both cortical ER (cER) and perinuclear ER (pnER) in WT cells (**Fig S1A-B**) (Chao, Piña, and Niwa, 2021).

The SARS-CoV-2 Nsp4 gene was placed under a galactose promoter in a yeast 2μ overexpression plasmid which was then used to transform into the yeast cells. Upon induction of Nsp4 expression by shifting a minimum synthetic media (-URA) containing 2% raffinose (-Gal) to that with 2% galactose (+Gal) for 3 hours at 30 °C, we analyzed the impact of Nsp4 expression on the ER morphology in live cells under a fluorescent deconvolution microscope. The nuclear DNA was visualized by staining with 4′,6-diamidino-2-phenylindole (DAPI), allowing us to clearly mark the nucleus. In agreement with previous reports by us and others (Chao, Piña, and Niwa, 2021; Voeltz, Rolls, and Rapoport, 2002), the Pho88-GFP reporter allowed us to visualize both the cER under the cortex of the mother cell membrane and the pnER, encircling the DAPI

stained nuclear DNA (**Fig S1A-B**). Upon expression of Nsp4 by shifting the growth medium to that with the Gal-containing media (+Gal) for 3 hrs, the overall morphologies of both pnER and the cER was significantly altered **(Fig 1A).** Furthermore, relatively uniform distributions of Pho88-GFP throughout the ER, both the pnER and the cER, were lost upon Nsp4 expression. Significantly, we found that the overall morphology of the pnER was altered, as it changed from a smooth round nuclear shape to deformed shapes with occasional deposits of higher levels of GFP in some areas **(Fig 1A and C, white arrowheads)**. Taken together, these results revealed that expression of Nsp4 alone can cause the ER morphological changes that may contribute to the formation of DMVs when cells are infected by SARS-CoV-2 virus. Interestingly, expression of Nsp6 results in the ER morphological changes distinct from those caused by Nsp4 (data not shown), suggesting that the DMV is formed by distinct morphological changes induced by each Nsp gene and may retain a unique function.

Nsp4-induced pnER morphological changes occur independent of UPR or ERSU components

Identification of host genes will provide the first step towards understanding the molecular mechanisms involved in the DMV formation. Since DMVs are produced from the ER membrane, we reasoned that Nsp4-induced morphological changes of the ER may involve previously characterized signaling pathways, such as UPR or ERSU pathways. We examined potential roles of the UPR by expressing Nsp4 into yeast cells lacking an UPR initiating component, Ire1 (*ire1Δ* cells). We hypothesized that if the UPR is involved, Nsp4 expression in *ire1Δ* cells should diminish the Nsp4-induced ER morphological changes. Overall ER morphological changes were observed in *ire1Δ*

cells at the extent similar to Nsp4 expression in WT cells (**Figure 2A-B, white arrowheads**). Furthermore, Nsp4 expression in cells that lack an ERSU component, Slt2 (*slt2Δ* cells), also induced the morphological ER changes observed in Nsp4 expressed WT cells **(Figure 2C and 2A, white arrowheads).** Taken together, these results suggest that Nsp4 dependent morphological changes of the ER are mediated by components beyond the UPR and the ERSU pathway.

Nsp4 expression leads to the cER inheritance block

In addition to the ER morphological changes, we noted that daughter cells had almost no cER upon Nsp4 expression when shifting cells into a galactose containing growth media **(Fig 3A).** Previously, we characterized the ERSU cell cycle checkpoint that ensures the inheritance of functional ER during the yeast cell cycle (Babour *et al.*, 2010). Specifically, in response to ER stress, we found that the cER entry to the daughter cell is diminished. We also found that the septin ring becomes mislocalized from the bud neck to a location of previous cell division known as the cytokinetic remnant (CRM), ultimately leading to the cytokinesis block in yeast and preventing generation of cells with non-functional ER.

To this end, we quantitated the cER inheritance into the daughter cell in a manner we established previously (Babour *et al.*, 2010). The bud index (ratio between mother and daughter cell diameter) was used to group cells into three classes, Class I, II, and III, depending upon cell cycle stages.

Early in the cell cycle in Class I cells, we found that Nsp4 expression caused nearly 70% of WT daughter cells to lack cER (**Fig 3A-B, Class I (+Gal)**). Strikingly, 75-80% of daughter cells also lacked the cER later in the cell cycle of Class II or III

cells (**Fig 3A-B, Class II and III (+Gal)**). This was in stark contrast to the cER inheritance block observed with ER stress induced by tunicamycin (Tm), a glycosylation inhibitor that induces ER proteotoxic stress.

Upon Tm treatment, the cER inheritance block was most significant with Class I cells and occurred at 40%, while less pronounced in Class II and III cells at ~55% and ~80% respectively **(Fig S2A and C)**, in agreement with the trend that was reported in our earlier publications (Babour *et al.*, 2010; Chao, Pina, and Niwa, 2021).

In addition, the daughter cells with Nsp4 expression sometimes contained a complete lack of the cER or had smaller fragments of the cER, even though the overall levels of the cER in the daughter cell still remained less than 20% (**Fig 3A**).

It should be mentioned that the observed difference of the cER inheritance was unlikely to be caused by the use of different sugars (raffinose, galactose or dextrose). We performed Tm treatment of WT cells grown in media containing 2% raffinose or dextrose and found that the extent of the cER inheritance block occurred at similar levels (**Fig S2A-D**). Thus, these results revealed that the increased level of the cER inheritance block in Nsp4 expressed cells was unlikely to be caused by differences in the sugar used in the growth medium, but rather inherent to Nsp4 expression.

In addition to the ER stress induced cER inheritance block, we tested another ERSU hallmark event, mislocalization of the septin ring from the bud neck to the CRM using Nsp4 expressed cells carrying a genomically integrated GFP tagged form of the Shs1 septin subunit (Shs1-GFP) into the genomic *shs1* locus (Chao *et al.*, 2019). The CRM was visualized by staining with calcofluor white (CW). We found that Tm addition into cells grown in raffinose (no Nsp4 expression) resulted in ~40%

mislocalization of Shs1-GFP (green) from the bud neck to the CRM (red) (**Fig 3C-D and G**). Like the cER inheritance block, these results in raffinose are in good agreement with the septin ring mislocalization observed in Tm treated cells grown in the dextrose containing media (Chao *et al.*, 2019). Expression of Nsp4 in the galactose containing media showed an increase in the Shs1-GFP mislocalization, albeit to a lesser extent when compared to Tm treatment **(Fig 3E and G)**. When Tm and Nsp4 expression were combined, the extent of the Shs1-GFP mislocalization increased to ~65%, additive of Tm and Nsp4 expression **(Fig 3F and G).** Interestingly, while a majority of the septin rings displayed mislocalization to the CRMs, we also observed some distinctive Shs1-GFP foci localized outside of the bud neck and the CRMs **(Fig 3E)**. Together, Nsp4 expression resulted in the activation of the ERSU molecular events, the ER inheritance block and septin mislocalization, although details of the ERSU activation modes differed from those induced by canonical proteotoxic ER stress inducers such as tunicamycin.

Nsp4-induced cER inheritance block occur independent of ERSU and UPR components

Previously, we reported that the ERSU components, such as Slt2, mediate ER stress and induce the ERSU hallmark events such as the ER inheritance block and septin ring mislocalization, independent of the UPR signaling pathway (Barbour *et al.*, 2010). Given the distinct nature of the Nsp4-induced cER inheritance block observed, we tested if the cER inheritance block occurred by the UPR or the ERSU pathways in Nsp4 expressing *ire1Δ* or *slt2Δ* cells. Tm-induction of *slt2Δ* cells grown in dextrose containing media failed to show the cER inheritance block. 25%, 50%, and 85% of

Class I, II and III *slt2Δ* cells, respectively, displayed cER inheritance as anticipated from the ERSU deficient cells (**Fig S3B and D;** Barbour *et al.,* 2010). In contrast, *ire1Δ* cells grown in dextrose containing media and treated with Tm resulted in cER inheritance block similar to that of Tm-induced WT cells. Class I, II, and III cells had ~60%, 80% and 85% cER inheritance block comparable to WT cells able to initiate the ERSU pathway **(Fig S3A and C).** These were consistent with our previously reported results, demonstrating that Slt2 plays a role in the Tm-induced cER inheritance block in ERSU pathway whereas Ire1 does not.

Surprisingly, *slt2Δ* cells did not impact the cER inheritance by Nsp4 expression: only ~23% of *slt2Δ* cells showed the cER inheritance in all three classes of cells at the extent similar to Nsp4 expressed WT cells (~25%) (**Fig 4B and D**). In addition, Nsp4 expression in *ire1Δ* cells also blocked the cER inheritance (~23%) at the level similar to that in WT cells (~25%), throughout the cell cycle **(Fig 4A and C)**.

Together, these results suggest that neither Slt2 nor Ire1 are not involved in a unique cER inheritance block caused by Nsp4 and differs from canonical ER stress induced cases.

Nsp4-induced ER morphological changes are mediated by ESCRT proteins, Vps4 and Vps24.

One of the major strengths of establishing a minimum experimental system to study SARS-CoV-2 DMV formation would be the identification of host genes involved in the ER morphological changes that lead to the DMV formation. Towards this goal, we first aimed to identify host genes that play a significant role in the ER morphological changes ultimately resulting in the DMV formation. As an initial step prior to genome-

wide comprehensive searches for host genes involved, we tested some candidate genes based on the knowledge of the genes. Specifically, we reasoned that genes known to be involved in membrane bending and scission might make good candidates as such functions are likely to be involved in the DMV formation.

Among several candidates, we focused on testing the involvement of the genes coding for the endosomal sorting complexes required for transport (ESCRT) as potential candidate genes including Vps4, Vps24 Vps23, and Snf7. In *S. cerevisiae*, at least five ESCRT genes have been reported to catalyze various cellular processes that involve unique membrane remodeling events, such as multivesicular body (MVB) sorting, cytokinesis, and the release of some enveloped viruses from the infected host cell surface (Raiborg and Stenmark, 2009; Carlton, 2010; Chen and Lamb, 2008). While the roles of ESCRT proteins on the ER membrane have not been described, the recent finding that ESCRT might be involved in inner nuclear membrane phase separation during the reformation of the inner nuclear membrane suggested their potential involvement (von Appen *et al.*, 2020; Olmos *et al.*, 2015).

To this end, we transformed a regulatable Nsp4 expression plasmid into *vps4Δ* and *vps24Δ* cells and induced Nsp4 expression. We hypothesized that if an ESCRT protein were to be involved in the Nsp4-induced pnER morphology rearrangement phenotype, the deletion of that gene would result in pnER morphologies similar to that of cells with no Nsp4 expression. In raffinose, the morphologies of the pnER remained normal, similar to that in WT cells carrying a regulatable Nsp4 expression plasmid grown in raffinose **(Fig 5A-C)**. Upon shifting the growth medium containing galactose to express Nsp4, we observed morphologies of the cER and the pnER in *vps4Δ* and

vps24Δ cells remained mostly unchanged from those seen prior to Nsp4 expression **(Fig 5A-C, lack of white arrowheads)**. The distribution of pnER signal in the mother cell was overall uniform and circular, similar to the pnER found in cells without Nsp4 expression **(Fig 5B-C).** This retention of ER shape and lack of Pho88-GFP deposits near the nucleus was starkly different from Nsp4 expressing WT cells **(Fig 5A).** In contrast to *vps4Δ* and *vps24Δ* cells, the pER of *vps23Δ and snf7Δ* cells lost their uniform distribution of pnER in the mother cell, similar to Nsp4 expression in WT (**Fig 6A-B, white arrowheads).**

Taken together, these results suggested that Vps4 and Vps24 have partial morphological influence on pnER shape under the expression of Nsp4, while Vps23 and Snf7 do not.

Nsp4-induced cER inheritance block is mediated by Vps4, not Vps24, Vps23, and Snf7

We noted the morphological recovery of the Nsp4-induced pnER might also be correlated with the cER entry into the daughter cell. To determine if the lack of any of the ESCRT proteins diminishes the cER inheritance block, we examined the presence of the cER in individual ESCRT knockout daughter cells upon Nsp4 expression. In *vps4Δ* daughter cells, the numbers of the cells with the cER in the daughter cell were moderately increased **(Fig 7A-B, yellow arrowhead),** suggesting that Vps4 plays a role in the cER inheritance block in response to ER stress induced by expression of Nsp4 or Nsp4 like viral protein. The cells lacking the remaining three ESCRT genes, however, resulted in minimal to no cER inheritance into the daughter cell, similar to the phenotype observed in Nsp4 expressing WT cells **(Fig 8A-C, lack of yellow**

arrowhead). Interestingly, with Nsp4, ESCRT knockout cells for all three classes continued to display similar levels of the cER inheritance block similarly to what was observed for Nsp4 expressing WT cells **(Fig 7B, 8D-F).** Thus, we averaged the total number of daughter cells with cER inheritance and found that *vps4Δ* cells were able to inherit the cER in ~43% of cells, while *vps24Δ, vps23Δ,* and *snf7Δ* all had significantly diminished percentages of cells with cER inheritance **(Fig S4A).**

These results suggest, for the first time, that two specific ESCRT genes, Vps4 and Vps24, play a role in alterations of the ER membrane. Furthermore, Vps4, but not Vps24, impacted the ER inheritance into the daughter cell. Both Vps4 and 24 are associated with or subunits of the ESCRT-III complex, and thus, how the extent of the ER inheritance block into the daughter cell by Nsp4 expression was diminished only in *vps4Δ* cells, but not in *vps24Δ* cells remains elusive. In summary, recovery of the ER morphological changes is not sufficient to recover the ERSU ER inheritance block.

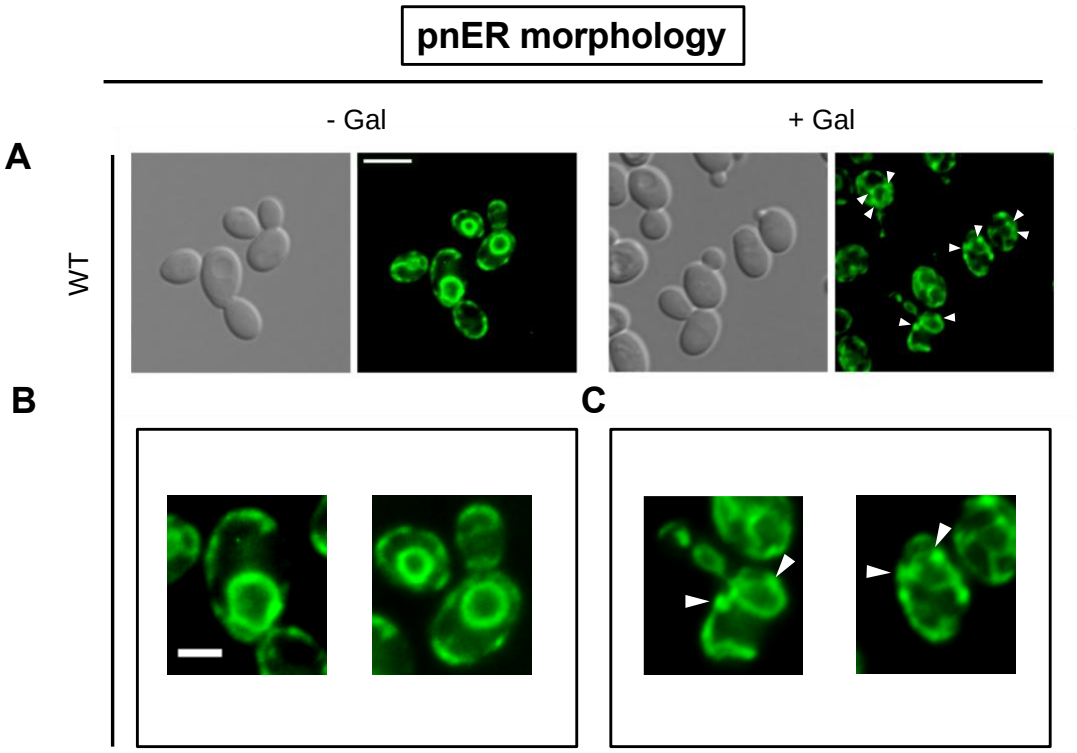

Figure 1: SARS-CoV-2 Nsp4 expression leads to significant changes in host ER membrane alteration

A) Differential interference contrast (DIC) and fluorescence microscopy of Pho88-GFP–expressing WT BY4741 cells in the absence (left) and presence (right) of SARS-CoV-2 nonstructural protein 4 (Nsp4). A plasmid carrying SARS-CoV2 Nsp4 was placed under a galactose-inducible promoter. Upon transformation of said plasmid, cells were grown in selective media (-URA) containing 2% raffinose. For expression of Nsp4, 2% galactose (+ Gal) was added to the cell culture to induce expression for 3 hours. 1.5 mL of cells were then collected for live microscopic observation. Each experiment inducing Nsp4 in this study will be performed with the above methodologies. Scale bar, 5μm.

B) Zoomed images of ER (Pho88-GFP) in WT cells transformed with Nsp4 plasmid but not expressed (-Gal). Scale bar, 2μm.

C) Zoomed images of ER (Pho88-GFP) in WT cells expressing Nsp4 (+Gal). White arrowheads indicate the presence of Pho88-GFP deposits. Scale bar, 2μm.

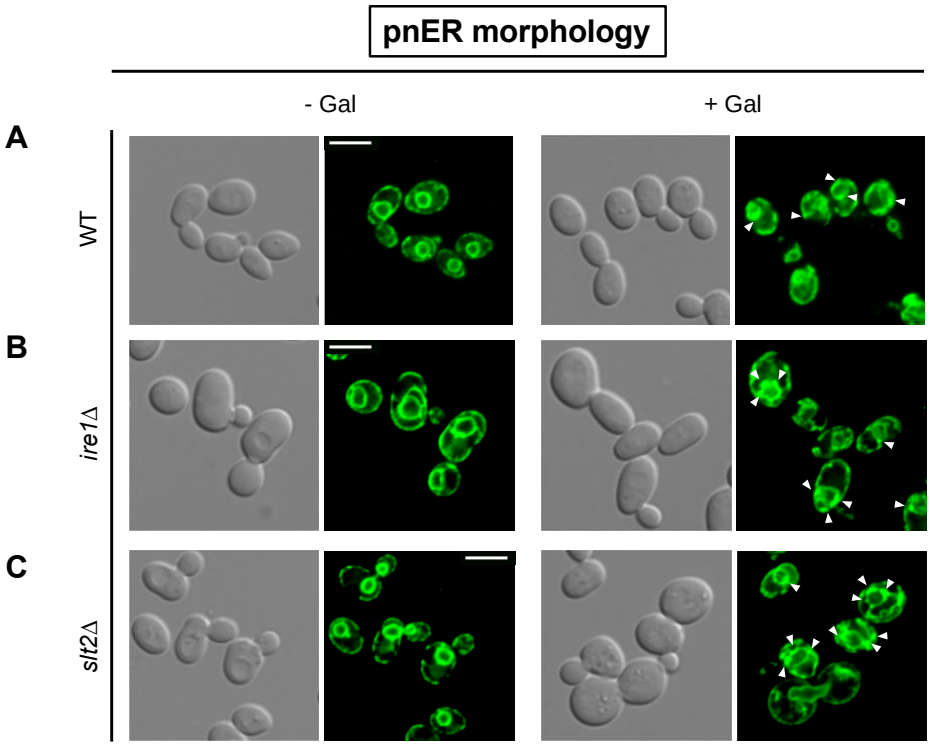

Figure 2: Nsp4-induced pnER morphological changes occur independent of UPR or ERSU components

A-C) DIC and GFP fields of Pho88-GFP expressing WT (A), *ire1Δ* (B), and *slt2Δ* (C) cells in the absence (left) and presence (right) of Nsp4 expression. White arrowheads indicate the presence of Pho88-GFP deposits. All scale bars, 5μm.

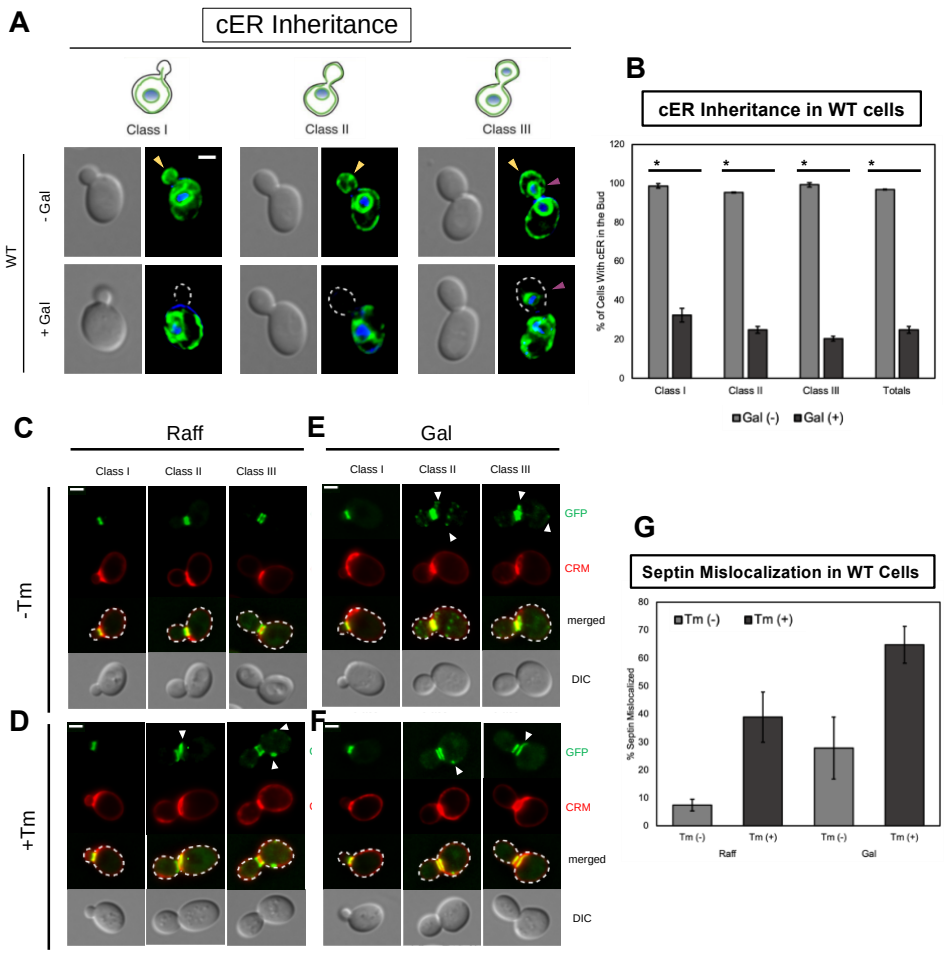

Figure 3: Nsp4 expression leads to the cER inheritance block and septin translocation

A) Individual DIC and GFP-DAPI merged images of ER (Pho88-GFP) in WT cells in the absence (above) and presence (below) of Nsp4. Cell Class was determined by the bud index (ratio of daughter to mother cell diameters). Class I cells had a bud index of 0-0.333, while Class II and Class III cells had a bud index of 0.333-1, with or without pnER, respectively. Yellow arrowheads indicate cER in the daughter bud, and magenta arrowheads indicate pnER in the daughter bud. Each merged GFP-DAPI image lacking cER in the daughter cell has the position of the cell surface membrane traced with a white dotted line. All scale bars, 2μm.

B) Quantitation of Class I, II, and III WT daughter cells containing cER. Data shown are the mean ± SD of three independent experiments (n >150 cells of each strain and treatment). ** indicates $p < 0.05$ and * indicates $p < 0.01$.

C-F) Individual WT BY7043 cells expressing Shs1-GFP (green). Calcofluor white (CW) staining highlights the cytokinetic remnants (CRMs, red). Each GFP-CRM merged image has the position of the cell surface membrane traced with a white dotted line. Cells in C and E were treated with DMSO (-Tm), while cells in D and F were treated with tunicamycin (+Tm). Nsp4 expression was not induced (left, Raff) or induced (right, Gal). Septin mislocalization is indicated by a white arrowhead. Class was divided by the bud index as follows: Class I (0-0.333), Class II (0.333-0.666), and Class III (0.666-1). All scale bars, 2μm.

G) Quantitation of total WT Shs1-GFP cells with septin mislocated away from the bud neck. Data shown are the mean ± SD of two independent experiments (n >150 cells of each strain and treatment).

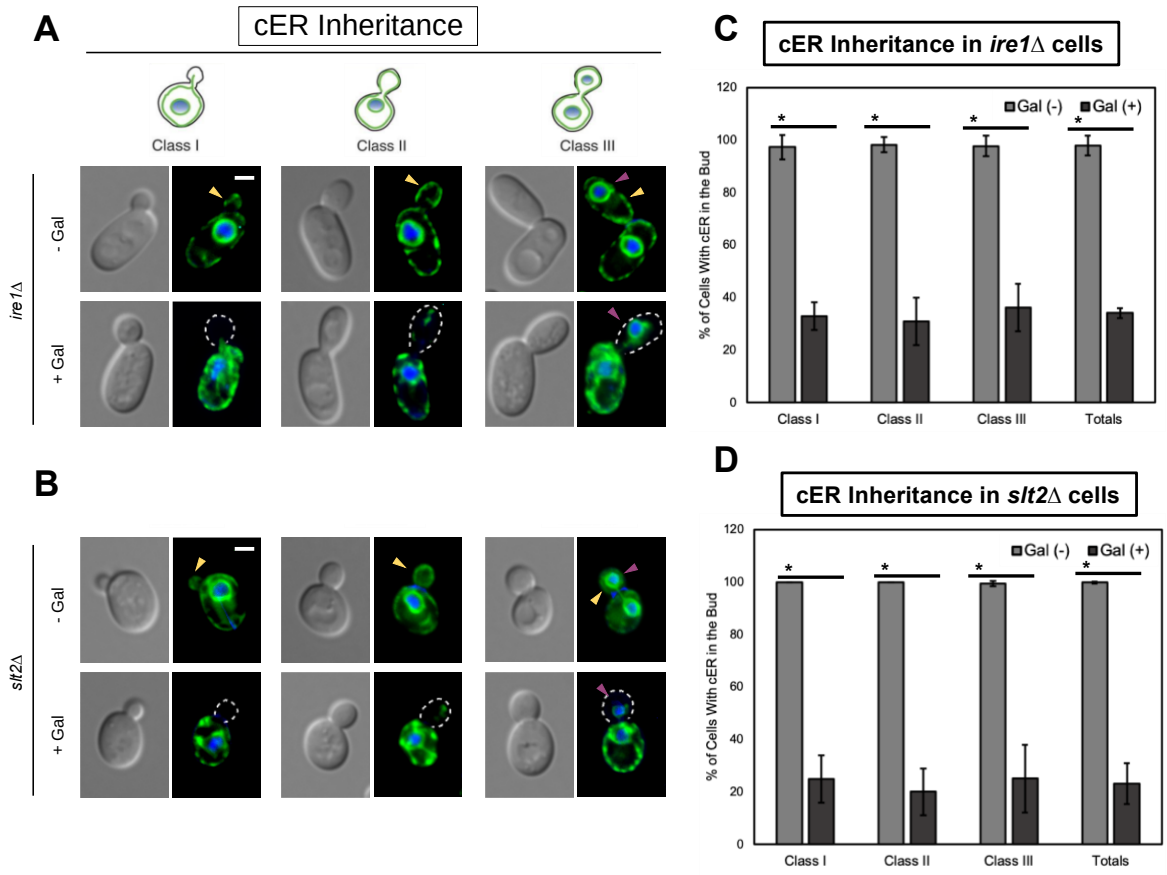

Figure 4: Nsp4-induced cER inheritance block occurs independent of UPR or ERSU components

A-B) Individual DIC and GFP-DAPI merged images of ER (Pho88-GFP) in *ire1Δ* (A) and *slt2Δ* (B) cells in the absence (above) and presence (below) of Nsp4. Yellow arrowheads indicate cER in the daughter bud, and magenta arrowheads indicate pnER in the daughter bud. Each merged GFP-DAPI image lacking cER in the daughter cell has the position of the cell surface membrane traced with a white dotted line. All scale bars, 2μm.

C-D) Quantitation of Class I, II, and III WT daughter cells containing cER. Data shown are the mean ± SD of three independent experiments (n >150 cells of each strain and treatment). ** indicates $p < 0.05$ and * indicates $p < 0.01$.

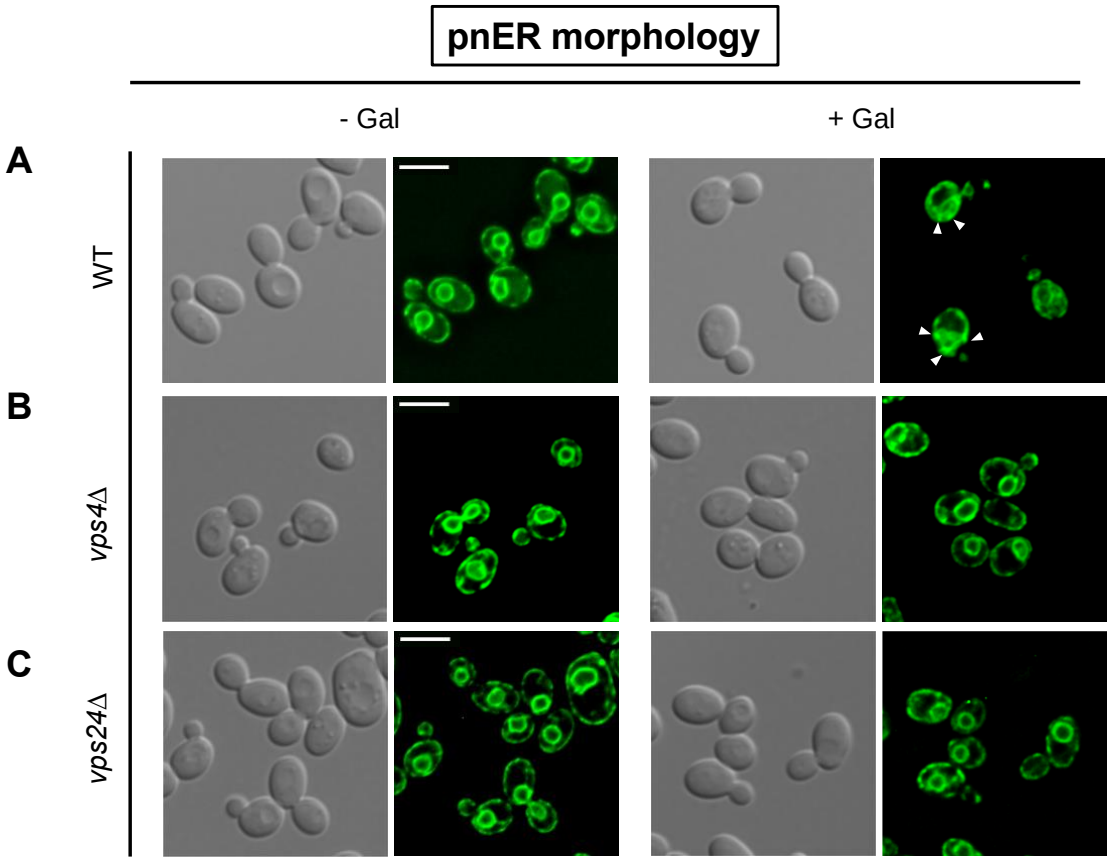

Figure 5: Nsp4-induced pnER morphological changes are mediated by ESCRT proteins Vps4 and Vps24

A-C) DIC and GFP fields of Pho88-GFP expressing WT (A), *vps4Δ* (B), and *vps24Δ* (C) cells in the absence (left) and presence (right) of Nsp4. White arrowheads indicate the presence of Pho88-GFP deposits. All scale bars, 5μm.

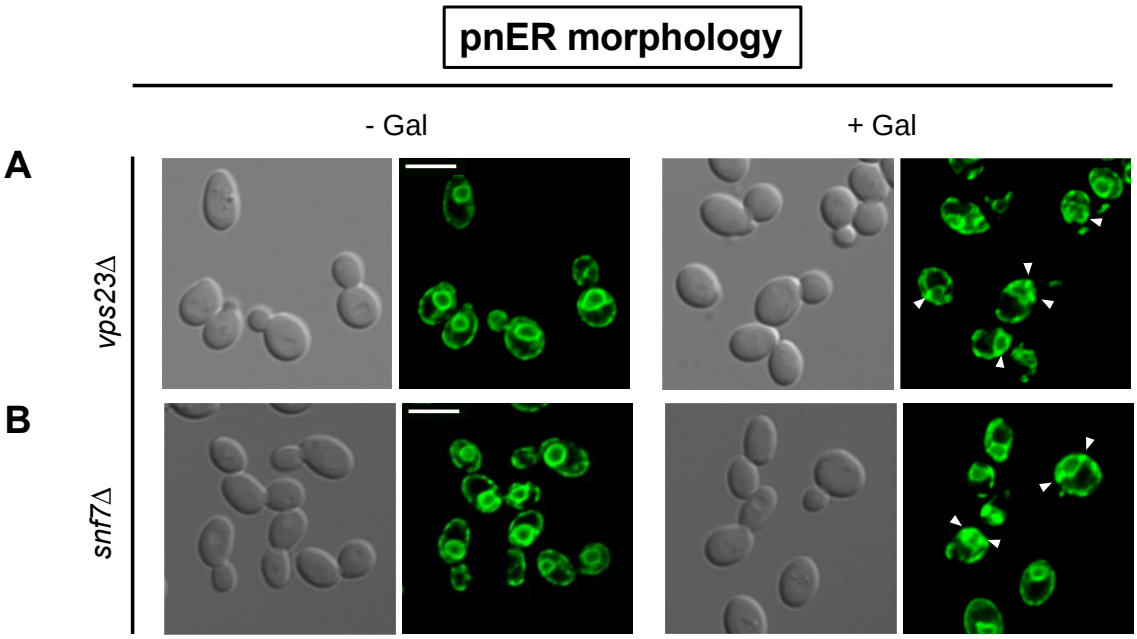

Figure 6: Nsp4-induced pnER morphological changes are not affected in knockout cells of Vps23 and Snf7

A-B) DIC and GFP fields of Pho88-GFP expressing *vps23Δ* (A) and *snf723Δ* (B) cells in the absence (left) and presence (right) of Nsp4. White arrowheads indicate the presence of Pho88-GFP deposits. All scale bars, 5μm.

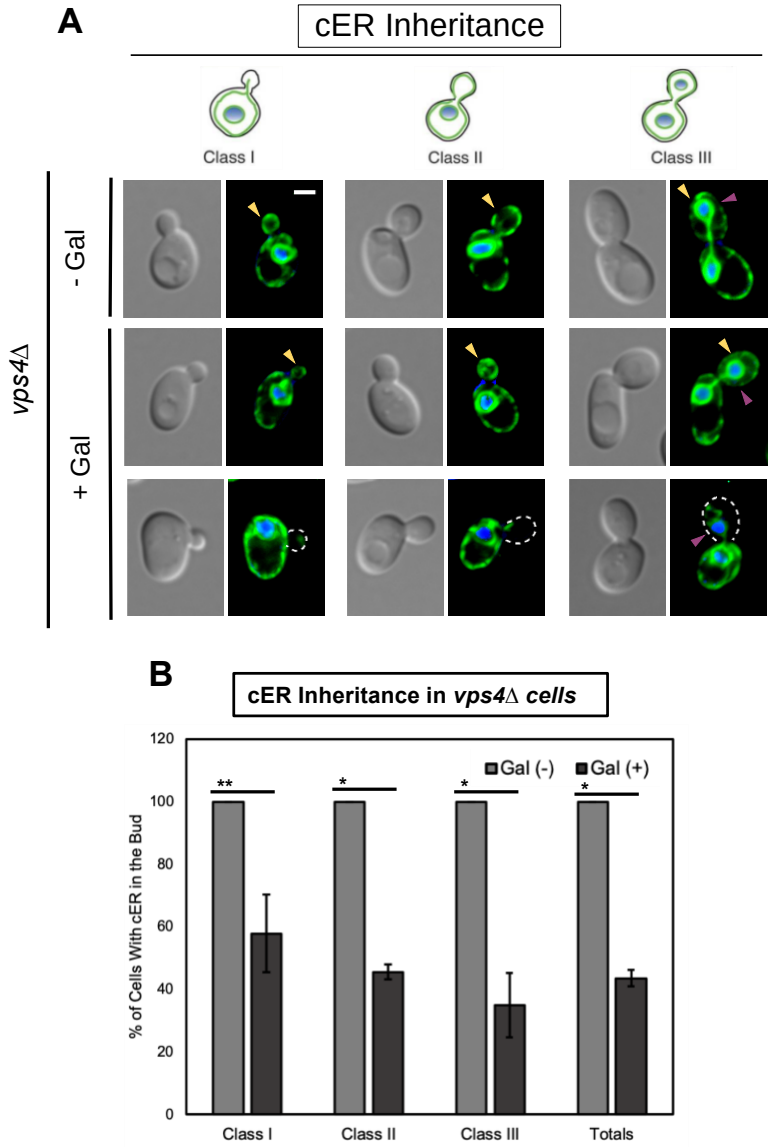

Figure 7: Nsp4-induced cER inheritance block is mediated by Vps4

A) Individual DIC and GFP-DAPI merged images of ER (Pho88-GFP) in *vps4Δ* cells in the absence (above) and presence (below) of Nsp4. Yellow arrowheads indicate cER in the daughter bud, and magenta arrowheads indicate pnER in the daughter bud. Each merged GFP-DAPI image lacking cER in the daughter cell has the position of the cell surface membrane traced with a white dotted line. Scale bar, 2μm.

B) Quantitation of Class I, II, and III WT daughter cells containing cER. Data shown are the mean ± SD of three independent experiments (n >150 cells of each strain and treatment). ** indicates $p < 0.05$ and * indicates $p < 0.01$.

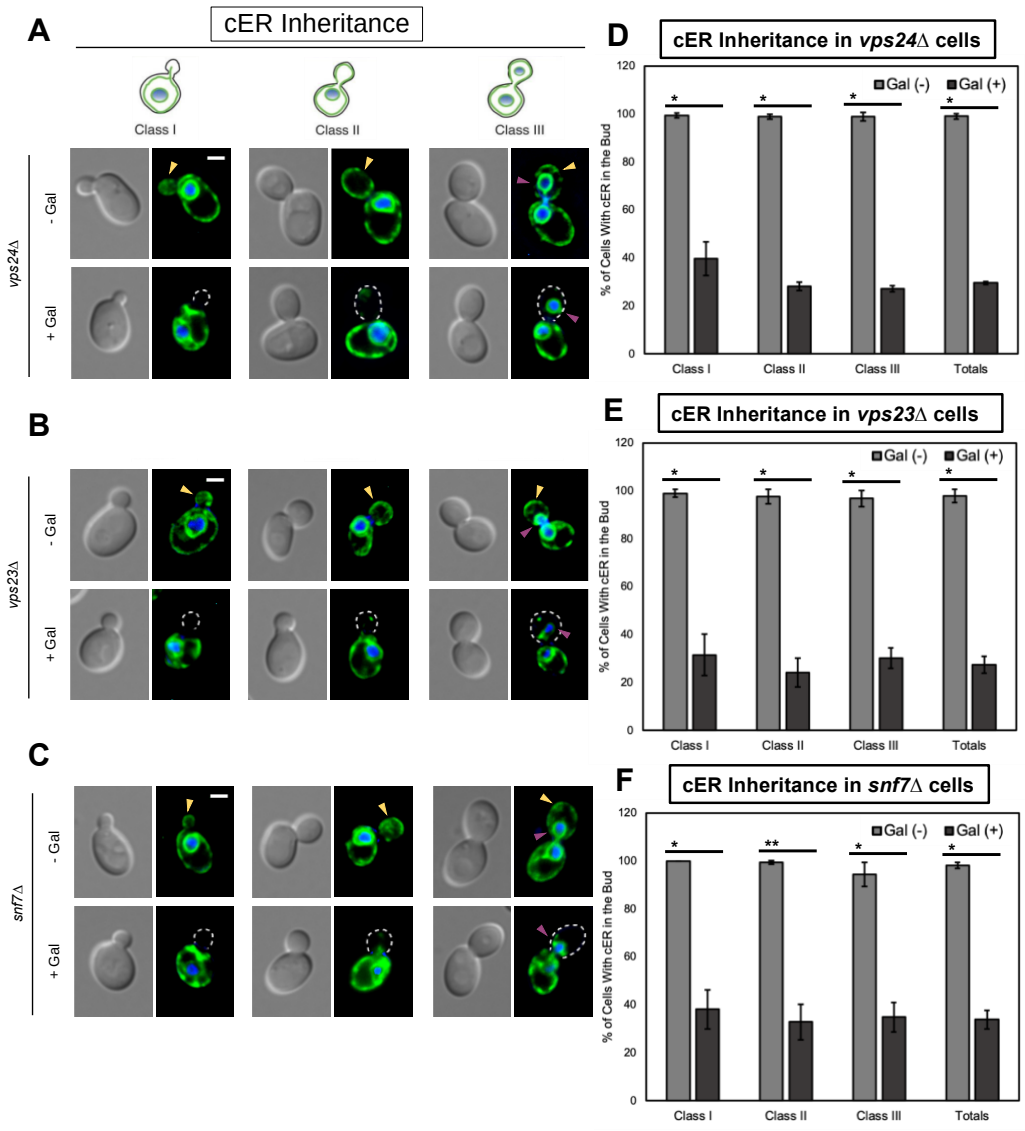

Figure 8: Nsp4-induced cER inheritance block is not mediated by Vps24, Vps23 and Snf7

A-C) Individual DIC and GFP-DAPI merged images of ER (Pho88-GFP) in *vps24Δ*, *vps23Δ*, and *snf7Δ* cells in the absence (above) and presence (below) of Nsp4. Yellow arrowheads indicate cER in the daughter bud, and magenta arrowheads indicate pnER in the daughter bud. Each merged GFP-DAPI image lacking cER in the daughter cell has the position of the cell surface membrane traced with a white dotted line. Scale bar, 2μm.

D-F) Quantitation of Class I, II, and III WT daughter cells containing cER. Data shown are the mean ± SD of three independent experiments (n >150 cells of each strain and treatment). ** indicates $p < 0.05$ and * indicates $p < 0.01$.

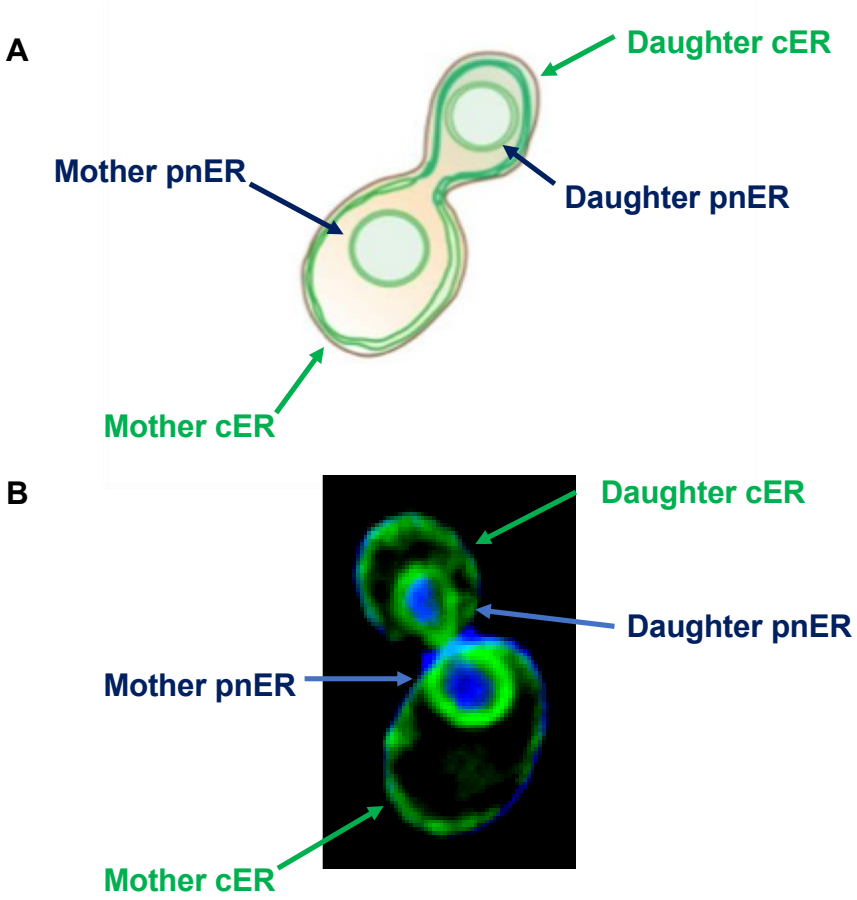

Figure S1: Endoplasmic reticulum (ER) structure in *S. cerevisiae* cells

A) Cartoon representation of ER structure in a dividing *S. cerevisiae* cell. The perinuclear ER (pnER) is contiguous with the nuclear membrane while the cortical ER (cER) lies under the plasma membrane.

B) Representative GFP image of ER structure in a dividing *S. cerevisiae* cell.

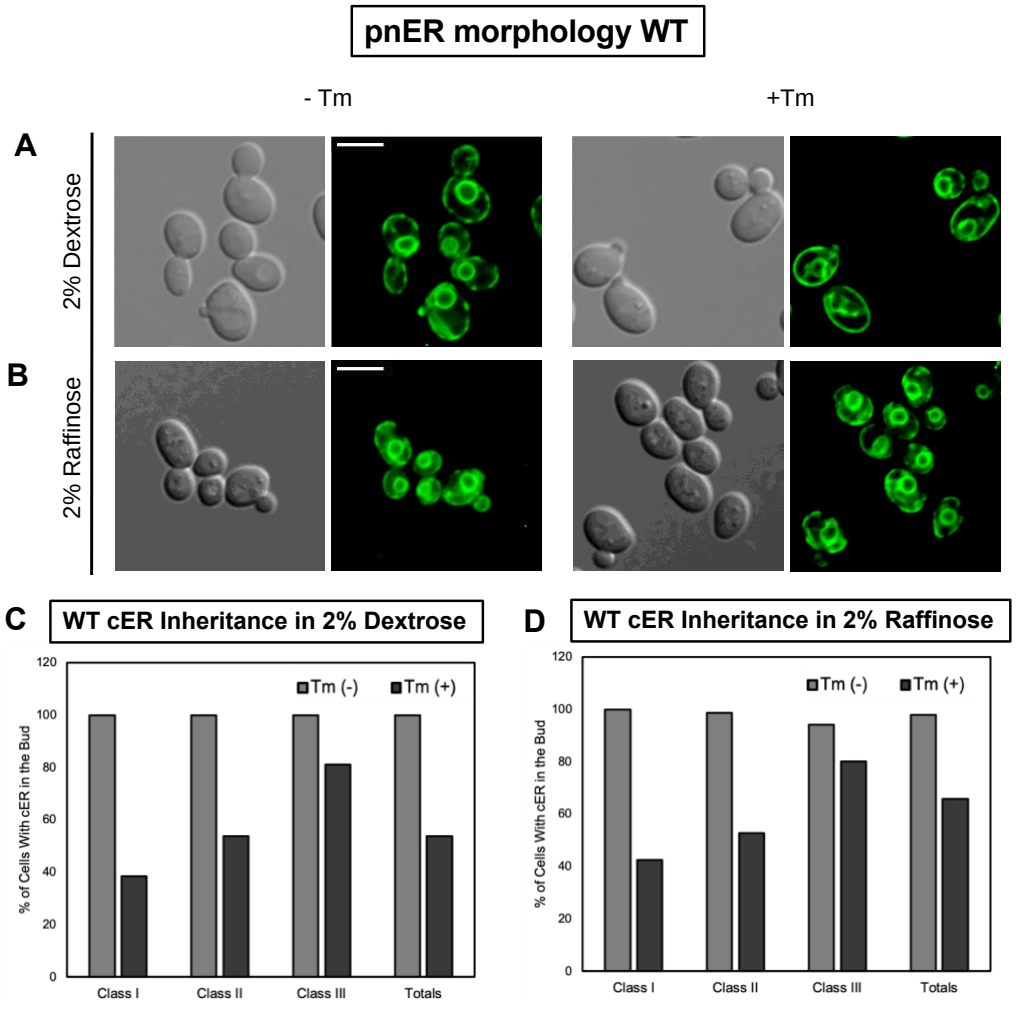

Figure S2: Different sugars used in growth media are not the cause of cER inheritance phenotype

A-B) DIC and GFP fields of WT cells expressing Pho88-GFP grown in 2% dextrose (above, A) and 2% raffinose (below, B). Cells were treated with DMSO (-Tm, left) and with Tm (+Tm, right) to induce ER stress. All scale bars, 5μm.

C-D) Quantitation of Class I, II, and III WT daughter cells containing cER and grown in 2% dextrose (C) and 2% raffinose (D). Data shown are derived from one repeat (*n* >150 cells of each strain and treatment).

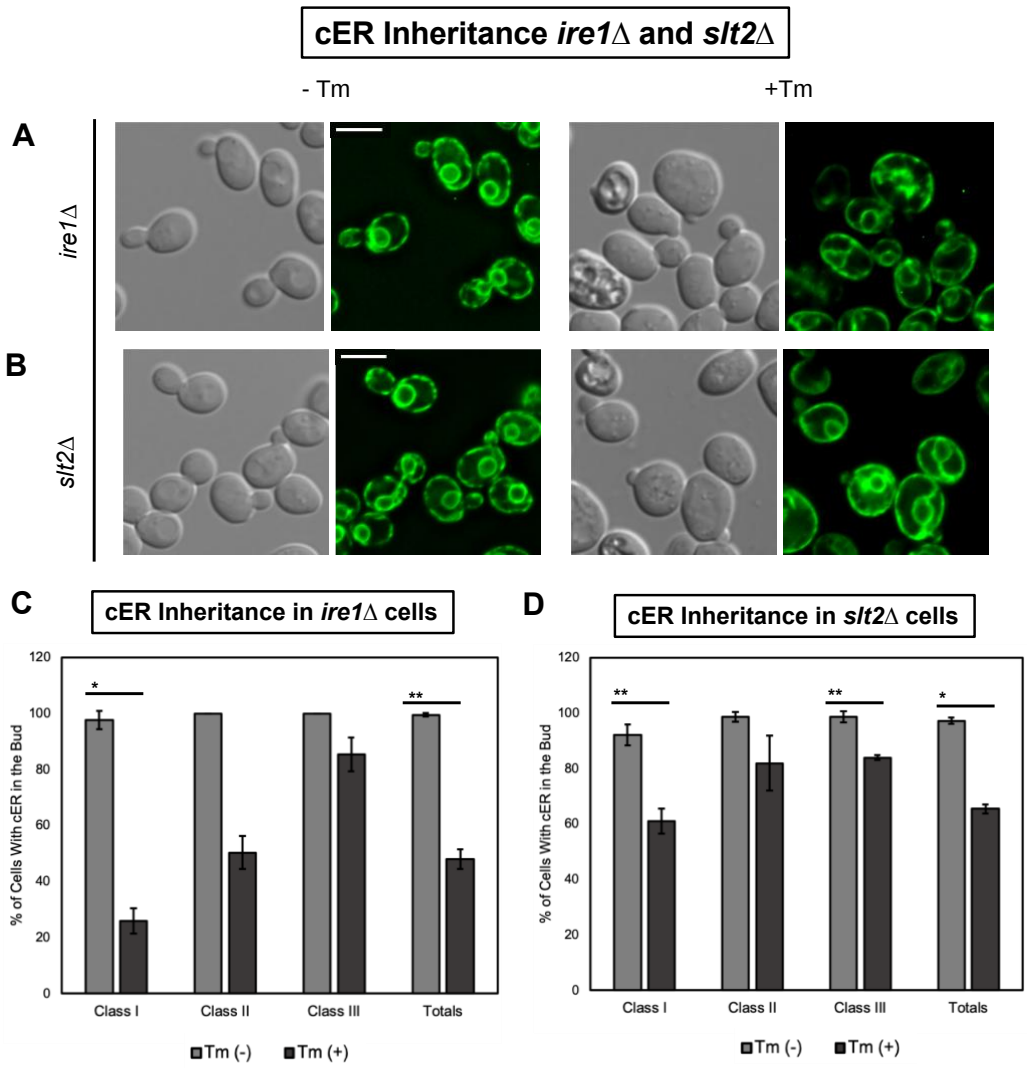

Figure S3: ER stress induced cER inheritance block occurs dependent on Slt2 not Ire1

A-B) DIC and GFP fields of *ire1Δ* (A) and *slt2Δ* cells expressing Pho88-GFP treated with DMSO (-Tm, left) and with Tm (+Tm, right) to induce ER stress. Cells were grown in 2% dextrose containing media. All scale bars, 5μm.

C-D) Quantitation of Class I, II, and III WT daughter cells containing cER. Data shown are the mean ± SD of two independent experiments (n >100 cells of each strain and treatment). ** indicates $p < 0.05$ and * indicates $p < 0.01$.

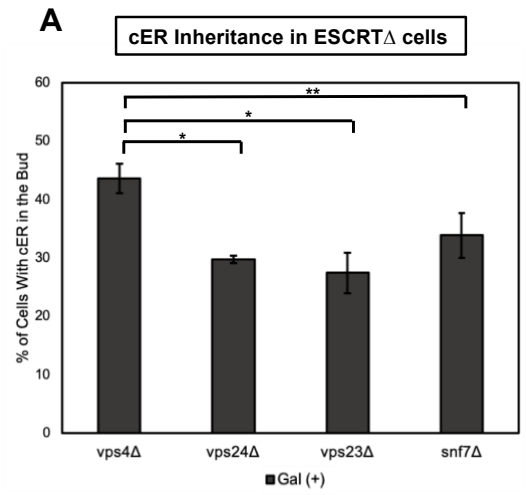

Figure S4: cER inheritance is primarily mediated by Vps4

A) Quantitation of total *vps4Δ*, *vps24Δ*, *vps23Δ* and *snf7Δ* daughter cells containing cER under Nsp4 expression (+Gal). Data shown are the mean ± SD of three independent experiments (n >150 cells of each strain and treatment). ** indicates $p < 0.05$ and * indicates $p < 0.01$.

DISCUSSION

In this Thesis, we sought out to understand the role of host cell components and the molecular mechanisms by which the ER is rearranged under SARS-CoV-2 Nsp4 expression. Using a minimum experimental system, we demonstrated that expression of one of the ER localized Nsps of SARS-CoV-2 is sufficient to cause major morphological changes in the ER. We found that genes encoding for important UPR and ERSU upstream elements were not involved in the pnER morphology change. Interestingly, we observed that the ERSU hallmark events, the ER inheritance block and septin ring mislocalization, occurred in WT cells with Nsp4 expression, indicating that the ERSU pathway was activated. Surprisingly, cER inheritance block was not controlled by neither the UPR nor the ERSU upstream elements. Additionally, we found that among the proteins integral for the ESCRT pathway, Vps4 and Vps24 mediated Nsp4 induced pnER morphology changes. While Vps4 and Vps24 have unique roles in pnER morphology changes, Vps4 alone influenced Nsp4 induced cER inheritance block. Together, our results suggest that expressed Nsp4 along with host proteins differentially results in ER functional demands, structural rearrangements and ER stress pathways responses.

The ER is a large, dynamic organelle with a reticular structure composed of both proteins and lipids (Voeltz, Rolls, and Rapoport, 2002). We see that canonical ER stress derived from the cell can cause structural changes, such as the overexpression of ER transmembrane and luminal proteins (proteotoxic stress). While an increased need to translate and modify proteins is one way to induce ER stress, ER functional capacity can also be surpassed by increasing lipid synthesis or reducing calcium storage levels.

To account for an increased demand for proteins and lipids, the UPR increases the size of the ER and thus increases the functional capacity of the cell. In many cases, this UPR-induced increase in ER proliferation is classified as a "ER structural change" and is not distinguished from a true morphology change.

In an example where morphological changes were differentiated, the overexpression of 3-hydroxy-3-methylglutaryl coenzyme A (HMG-CoA) reductase resulted in the activation of the UPR, thus leading to ER expansion to accommodate for increased proteome demand (Wright *et al.,* 1988). However, independent of the UPR, HMG-CoA overexpression induced the formation of karmellae, which are stacks of proliferated ER wrapped around the nucleus. Thus, it is important to distinguish the ER structural changes induced by Nsp4, as the UPR-induced proliferation of ER is distinctively different from that of the pnER morphology change, suggesting that viral proteins carry unique features that impact ER lipids. Even less understood is how these structures are inherited during cell division.

This same approach of separating ER functional capacity, morphology changes, and inheritance is useful to apply to our minimal approach. Additionally, reducing the complexities of DMV formation by intact viruses to a minimal expression of a single ER-associated Nsp protein provides a bottoms-up approach leading to the understanding of the complexities of DMV formation and viral-host protein interactions. Currently, as the intermediate stages of DMV formation is largely unclear, we may gain better insight into where specific characteristics are originating from, via single ER-associated Nsp expression.

Considering that we are essentially overexpressing a viral nonstructural protein and thus causing proteotoxic stress, it made sense that we also observed the ERSU hallmark events of cER inheritance block and septin ring translocation. However, while these results implicated the involvement of the UPR and ERSU pathways, these ER-stress mitigating elements did not affect the ER morphology change induced by Nsp4. This further emphasizes the distinction between ER proliferation to accommodate functional demands compared to morphological changes of the ER membrane.

While the deletion of Slt2, the upstream ERSU element, did not cause an ERSU-deficient response, it is still possible that Nsp4 does engage with the ERSU pathway. Like many signaling pathways, the ERSU checkpoint has downstream activating elements, such as the binding and recognition of sphingolipids with reticulons, transmembrane proteins important for stabilizing ER curvature (Westrate *et al.*, 2015). It was previously thought that reticulon-sphingolipid binding fully controlled the ERSU pathway; however, a recent study suggested that reticulons may bind to other cellular factors beyond sphingolipids (Piña *et al.*, 2018). While the mutation of a single amino acid residue in the sphingolipid binding domain of a reticulon resulted in no cER inheritance block, the septin ring still translocated to the bud scar, rather than stay retained at the bud neck (Niwa, 2020). After the full deletion of the reticulon protein, cells were deficient in both ERSU events, suggesting that the reticulon contained a separate domain to independently control cER inheritance block and septin translocation (Piña *et al.*, 2016). These experiments provide evidence that reticulons have multiple domains and interactions in order to activate ERSU events. Thus, future

experiments exploring the relationship between viral ER-associated proteins and reticulons will be an interesting avenue.

In addition to the proteins involved in the ER stress response, the endosomal sorting complex required for transport (ESCRT) pathway is an intriguing host protein target for ER rearrangement. The ESCRT pathway is responsible for a variety of cellular functions, including enveloped viral budding, vesicle formation and transportation of cargo destined for endosomal degradation, and the abscission or detachment stage of cytokinesis (McCullough, Colf, and Sundquist, 2013). For each of these functions, ESCRT proteins are involved in remodeling the associated membrane, such as the nuclear envelope, endosomal membrane, and the plasma membranes respectively (Hurley, 2015). Given the ability of ESCRT proteins to deform and restructure cellular membranes, ESCRT proteins are additionally involved in retroviral budding and the formation of viral replication complexes of enveloped RNA viruses (Chen and Lamb, 2008; Shulla and Randall, 2016).

Thus, Vps4 and Vps24 may provide similar functions when ER structural changes are induced by viral proteins like Nsp4. In budding yeast, the nuclear envelope stays intact and does not break down during cell division. Thus, retaining the proper structure and quality of nuclear complexes, such as the nuclear pore complex (NPC), is important. It was identified in an epistatic screen in yeast that ESCRT III subunits and Vps4 are important for NPC structural quality control (Webster *et al.*, 2014). Rather than recruitment for upstream ESCRT factors, it appears that factors from the nucleus directly recruit ESCRT III. It is proposed that due to its disassembly abilities, the AAA ATPase Vps4 might serve to unfold and extract structurally unfavorable parts of the

NPC to maintain nuclear quality control (Yang *et al.*, 2015). Thus, Vps4 and Vps4 of the ESCRT III complex have genetic interactions with the nuclear pore complex (Webster *et al.,* 2014). As the pnER is maintained with the outer nuclear membrane, this might provide a reasonable explanation as to why Vps4 and Vps24 aid in mediating the pnER morphology changes observed in Nsp4 expressed cells. Typically, the recruitment of ESCRT III and Vps4 occur via upstream ESCRT complexes, such as ESCRT I and II (Adell *et al.,* 2017). However, since Vps4 and ESCRT III complexes are recruited to the NPCs by nuclear factors, rather than recruited by ESCRT factors, this may explain why proteins of ESCRT II like Vps23 are not involved in the ER rearrangements we observed (Webster *et al.,* 2014). Additionally, while Vps4 and Vps24 both are involved in Nsp4-induced ER morphology changes, Vps4 alone mediated cER inheritance. Once more, this result emphasizes the distinction that ER morphological changes and ER functional changes mediated by the UPR and ERSU pathways are separate phenotypes.

Our findings uncover a few of the unique roles that host proteins, that can canonically function to rearrange cellular membranes, play during ER-associated viral protein expression. Our model of single viral protein expression in a simplified model organism asks that complex viral structures like DMVs be broken down into how they affect the functional structure, rearranged morphology, and inheritance of targeted host organelles. Better differentiation of these unique observations will allow for a greater understanding of viral induced membrane rearrangements.

MATERIALS AND METHODS

Cell Strains:

The *S. cerevisiae* strains used in this Thesis are described in Table 1. Single-deletion strains with the KanMX marker originated from the yeast haploid deletion collection (BY4741, MAT a, Thermo Scientific). All ESCRT knockout Pho88-GFP strains were generated by amplifying the KanMX marker via a one-step standard PCR-based method and transforming the KanMX marker into WT Pho88-GFP MNY2661 (Longtine *et al.,* 1998b). This, in turn, created the knockout strains used in this Thesis.

Cells expressing Nsp4 (Table 1) were grown in synthetic complete -URA media containing yeast nitrogenous base, 2% raffinose and the appropriate amino acids for the genotype at 30°C and were examined live during log phase unless otherwise stated.

The Nsp4 plasmid (pGBW-m4046479) containing a URA auxotroph was obtained from AddGene (Table 3) and was transformed into all strains in Table 1.

Nsp4 Expression Assays

During mid-log phase, 2% galactose (+ Gal) or 2% raffinose (-Gal) was added to cell culture for 3 hours. 1.5 mL of cell culture were then collected, concentrated, and immediately imaged live via fluorescence microscopy.

Drug treatment

ER stress was induced upon addition of tunicamycin (Tm) (Calbiochem) at a final concentration of 1ug/mL at 30°C for 2 hours to analyze ER rearrangements. Tm (-) cells were treated with dimethyl sulfoxide (DMSO).

To visualize the nucleus and cytokinetic remnants (CRMs), we used DAPI (4′,6-diamidino-2-phenylindole) and 0.1µg/ml calcofluor white (CW) (Sigma) respectively. For cells stained with CW, cells were washed once with 1X PBS, incubated with CW for 2 minutes in the dark, and then washed once more with 1X PBS. Cells were imaged live immediately after staining.

Microscopy:

All live cells were visualized using an Axiovert 200M Carl Zeiss Micro-Imaging microscope with a 100x 1.3 NA objective. Images were captured using a monochrome digital camera (Axiocam; Carl Zeiss MicroImaging, Inc.) and analyzed using Axiovision software (Carl Zeiss MicroImaging, Inc.). Each image is a z-stack projection of 0.11µm intervals after constrained iterative deconvolution.

Quantifications and Statistical Analysis

The ImageJ software (National Institute of Health) was used for all quantifications. A minimum of 150 cells was measured for each experiment and each experiment was repeated three times, unless otherwise stated.

Progression through the cell cycle was determined by bud index (ratio of daughter and mother cell diameters) and is classified as follows: Class I cells (bud index of 0-0.333), Class II cells (bud index of 0.333-1 with no pnER divided into the daughter) and Class III cells (bud index of 0.333-1 with pnER divided into the daughter). Cell diameters were measured in ImageJ.

Daughter buds were scored for the inheritance of cER if GFP signal lined at least 80% or more of the bud cortex.

Quantitative data are expressed as mean ± SD. Student's 2 tailed T test was used to generate *p* values.

Table 1: Yeast Strains
Yeast strains utilized in this work. A list of yeast strains and the associated genotype used for experiments.

Strain Name	Genotype	Reference
BY4741	*MATa his3Δ1, leu2Δ0, met15Δ0, ura3Δ0*	Thermo Scientific
BY7092	*MATa can1Δ::STE2pr-Sp_his5, lyp1Δ, his3Δ1, leu2Δ0, ura3Δ0, met15Δ0*	Boone Lab
BY7043	*MAT alpha can1Δ::STE2pr-lue2 lyp1Δ his3Δ1 leu2Δ0 ura3Δ0 met15Δ0*	This Lab (FJP)
MNY2661	*BY4741 MATa his3Δ1, leu2Δ0, met15Δ0, ura3Δ0:: Pho88-GFP:HIS3*	This lab (JC)
MNY2817	*BY7092 MATa can1Δ::STE2pr-Sp_his5, lyp1Δ, his3Δ1, leu2Δ0, ura3Δ0, met15Δ0:: Pho88-GFP:HIS3, Ire1Δ::Nat*	This lab (JC)
MNY3167	*BY4741 MATa his3Δ1, leu2Δ0, met15Δ0, ura3Δ0:: Pho88-GFP:HIS3, ire1Δ::KanMX*	This lab (FJP)
A005	*BY4741 MATa his3Δ1, leu2Δ0, met15Δ0, ura3Δ0:: Pho88-GFP:HIS3, vps4Δ::KanMX*	This paper (AK)
A006	*BY4741 MATa his3Δ1, leu2Δ0, met15Δ0, ura3Δ0:: Pho88-GFP:HIS3, vps24Δ::KanMX*	This paper (AK)
A007	*BY4741 MATa his3Δ1, leu2Δ0, met15Δ0, ura3Δ0:: Pho88-GFP:HIS3, vps23Δ::KanMX*	This paper (AK)
A008	*BY4741 MATa his3Δ1, leu2Δ0, met15Δ0, ura3Δ0:: Pho88-GFP:HIS3, snf7Δ::KanMX*	This paper (AK)
MNY2662	*BY7043 MAT alpha can1Δ::STE2pr-lue2 lyp1Δ his3Δ1 leu2Δ0 ura3Δ0 met15Δ0:: Shs1-GFP:HIS3*	This lab (FJP)

Table 2: Primers.
Primers utilized in this work. A list of primers used to generate knockout cell lines.

Name	Sequence (5'-3')	Use
Vps4 upstream F	GATTTAATCGTGGGTTGAGGAC	Forward primer to make *vps4::KanMX*
Vps4 downstream R	CACCGCCGTTGTTAAAGTTAG	Reverse primer to make *vps4::KanMX*
Vps24 upstream F	TATGCTATACCAACAACTTTCATC	Forward primer to make *vps24::KanMX*
Vps24 downstream R	CTGTCTTTACCCTCACTATTACT	Reverse primer to make *vps24::KanMX*
Vps23 upstream F	GCGGAGAGAAGAGATTATGAC	Forward primer to make *vps23::KanMX*
Vps23 downstream R	CATTAGAAAGACTGGGTTAGTG	Reverse primer to make *vps23::KanMX*
Snf7 upstream F	CATGAATAGTTGGCAGAGCAG	Forward primer to make *snf7::KanMX*
Snf7 downstream R	CACATTCCCTTCTATACCTATG	Reverse primer to make *snf7::KanMX*

Table 3: Plasmids
Plasmids utilized in this work. A list of plasmids transformed into the yeast strains listed in Table 1 for the expression of viral Nps4 under the Gal promoter.

Plasmid Name	Construct	Reference
For Nsp4 ura3	pGBW-m4046479	pGBW-m4046479 was a gift from Ginkgo Bioworks & Benjie Chen (Addgene plasmid # 145495 ; http://n2t.net/addgene:145495 ; RRID:Addgene_145495)

REFERENCES

Adell, M. A. Y., Migliano, S. M., Upadhyayula, S., Bykov, Y. S., Sprenger, S., Pakdel, M., Vogel, G. F., Jih, G., Skillern, W., Behrouzi, R., Babst, M., Schmidt, O., Hess, M. W., Briggs, J. A., Kirchhausen, T., & Teis, D. (2017). Recruitment dynamics of ESCRT-III and Vps4 to endosomes and implications for reverse membrane budding. *ELife*, *6*, e31652. https://doi.org/10.7554/eLife.31652

Angelini, M. M., Akhlaghpour, M., Neuman, B. W., & Buchmeier, M. J. (2013). Severe acute respiratory syndrome coronavirus nonstructural proteins 3, 4, and 6 induce double-membrane vesicles. *MBio*, *4*(4), e00524-13. https://doi.org/10.1128/mBio.00524-13

Appenzeller-Herzog, C., & Hauri, H.-P. (2006). The ER-Golgi intermediate compartment (Ergic): In search of its identity and function. *Journal of Cell Science*, *119*(11), 2173–2183. https://doi.org/10.1242/jcs.03019

Botstein, D., & Fink, G. R. (2011). Yeast: An experimental organism for 21st century biology. *Genetics*, *189*(3), 695–704. https://doi.org/10.1534/genetics.111.130765

Carlton, J. (2010). The ESCRT machinery: A cellular apparatus for sorting and scission. *Biochemical Society Transactions*, *38*(6), 1397–1412. https://doi.org/10.1042/BST0381397

Chao, J. T., Pina, F., & Niwa, M. (2021). Regulation of the early stages of endoplasmic reticulum inheritance during ER stress. *Molecular Biology of the Cell*, *32*(2), 109–119. https://doi.org/10.1091/mbc.E20-08-0558

Chao, J. T., Piña, F., Onishi, M., Cohen, Y., Lai, Y.-S., Schuldiner, M., & Niwa, M. (2019). Transfer of the septin ring to cytokinetic remnants in er stress directs age-sensitive cell-cycle re-entry. *Developmental Cell*, *51*(2), 173-191.e5. https://doi.org/10.1016/j.devcel.2019.08.017

Chen, B. J., & Lamb, R. A. (2008). Mechanisms for enveloped virus budding: Can some viruses do without an ESCRT? *Virology*, *372*(2), 221–232. https://doi.org/10.1016/j.virol.2007.11.008

Cohen, S., Valm, A. M., & Lippincott-Schwartz, J. (2018). Interacting organelles. *Current Opinion in Cell Biology*, *53*, 84–91. https://doi.org/10.1016/j.ceb.2018.06.003

Cortese, M., Lee, J.-Y., Cerikan, B., Neufeldt, C. J., Oorschot, V. M. J., Köhrer, S., Hennies, J., Schieber, N. L., Ronchi, P., Mizzon, G., Romero-Brey, I., Santarella-Mellwig, R., Schorb, M., Boermel, M., Mocaer, K., Beckwith, M. S., Templin, R. M., Gross, V., Pape, C., … Bartenschlager, R. (2020). Integrative imaging reveals

sars-cov-2-induced reshaping of subcellular morphologies. *Cell Host & Microbe*, *28*(6), 853-866.e5. https://doi.org/10.1016/j.chom.2020.11.003

Fehrenbacher, K. L., Davis, D., Wu, M., Boldogh, I., & Pon, L. A. (2002). Endoplasmic reticulum dynamics, inheritance, and cytoskeletal interactions in budding yeast. *Molecular Biology of the Cell*, *13*(3), 854–865. https://doi.org/10.1091/mbc.01-04-0184

Fun, X. H., & Thibault, G. (2020). Lipid bilayer stress and proteotoxic stress-induced unfolded protein response deploy divergent transcriptional and non-transcriptional programmes. *Biochimica et Biophysica Acta (BBA) - Molecular and Cell Biology of Lipids*, *1865*(1), 158449. https://doi.org/10.1016/j.bbalip.2019.04.009

Gordon, D. E., Jang, G. M., Bouhaddou, M., Xu, J., Obernier, K., White, K. M., O'Meara, M. J., Rezelj, V. V., Guo, J. Z., Swaney, D. L., Tummino, T. A., Hüttenhain, R., Kaake, R. M., Richards, A. L., Tutuncuoglu, B., Foussard, H., Batra, J., Haas, K., Modak, M., … Krogan, N. J. (2020). A SARS-CoV-2 protein interaction map reveals targets for drug repurposing. *Nature*, *583*(7816), 459–468. https://doi.org/10.1038/s41586-020-2286-9

Hagemeijer, M. C., Monastyrska, I., Griffith, J., van der Sluijs, P., Voortman, J., van Bergen en Henegouwen, P. M., Vonk, A. M., Rottier, P. J. M., Reggiori, F., & de Haan, C. A. M. (2014). Membrane rearrangements mediated by coronavirus nonstructural proteins 3 and 4. *Virology*, *458–459*, 125–135. https://doi.org/10.1016/j.virol.2014.04.027

Hampton, R. Y., & Sommer, T. (2012). Finding the will and the way of ERAD substrate retrotranslocation. *Current Opinion in Cell Biology*, *24*(4), 460–466. https://doi.org/10.1016/j.ceb.2012.05.010

Hartenian, E., Nandakumar, D., Lari, A., Ly, M., Tucker, J. M., & Glaunsinger, B. A. (2020). The molecular virology of coronaviruses. *Journal of Biological Chemistry*, *295*(37), 12910–12934. https://doi.org/10.1074/jbc.REV120.013930

Hurley, J. H. (2015). escrt s are everywhere. *The EMBO Journal*, *34*(19), 2398–2407. https://doi.org/10.15252/embj.201592484

Hurst, L. R., & Fratti, R. A. (2020). Lipid rafts, sphingolipids, and ergosterol in yeast vacuole fusion and maturation. *Frontiers in Cell and Developmental Biology*, *8*, 539. https://doi.org/10.3389/fcell.2020.00539

Karagas, N. E., & Venkatachalam, K. (2019). Roles for the endoplasmic reticulum in regulation of neuronal calcium homeostasis. *Cells*, *8*(10), 1232. https://doi.org/10.3390/cells8101232

Klumperman, J., Locker, J. K., Meijer, A., Horzinek, M. C., Geuze, H. J., & Rottier, P. J. (1994). Coronavirus M proteins accumulate in the Golgi complex beyond the site of virion budding. *Journal of Virology*, *68*(10), 6523–6534. https://doi.org/10.1128/jvi.68.10.6523-6534.1994

Knoops, K., Kikkert, M., Worm, S. H. E. van den, Zevenhoven-Dobbe, J. C., van der Meer, Y., Koster, A. J., Mommaas, A. M., & Snijder, E. J. (2008). Sars-coronavirus replication is supported by a reticulovesicular network of modified endoplasmic reticulum. *PLoS Biology*, *6*(9), e226. https://doi.org/10.1371/journal.pbio.0060226

Kozutsumi, Y., Segal, M., Normington, K., Gething, M.-J., & Sambrook, J. (1988). The presence of malfolded proteins in the endoplasmic reticulum signals the induction of glucose-regulated proteins. *Nature*, *332*(6163), 462–464. https://doi.org/10.1038/332462a0

Longtine, M. S., Mckenzie III, A., Demarini, D. J., Shah, N. G., Wach, A., Brachat, A., Philippsen, P., & Pringle, J. R. (1998). Additional modules for versatile and economical PCR-based gene deletion and modification in Saccharomyces cerevisiae. *Yeast*, *14*(10), 953–961. https://doi.org/10.1002/(SICI)1097-0061(199807)14:10<953::AID-YEA293>3.0.CO;2-U

McCullough, J., Colf, L. A., & Sundquist, W. I. (2013). Membrane fission reactions of the mammalian escrt pathway. *Annual Review of Biochemistry*, *82*(1), 663–692. https://doi.org/10.1146/annurev-biochem-072909-101058

Miller, S., & Krijnse-Locker, J. (2008). Modification of intracellular membrane structures for virus replication. *Nature Reviews Microbiology*, *6*(5), 363–374. https://doi.org/10.1038/nrmicro1890

Mori, K. (2000). Tripartite management of unfolded proteins in the endoplasmic reticulum. *Cell*, *101*(5), 451–454. https://doi.org/10.1016/S0092-8674(00)80855-7

Niwa, M. (2020). A cell cycle checkpoint for the endoplasmic reticulum. *Biochimica et Biophysica Acta (BBA) - Molecular Cell Research*, *1867*(12), 118825. https://doi.org/10.1016/j.bbamcr.2020.118825

Olmos, Y., Hodgson, L., Mantell, J., Verkade, P., & Carlton, J. G. (2015). ESCRT-III controls nuclear envelope reformation. *Nature*, *522*(7555), 236–239. https://doi.org/10.1038/nature14503

Oudshoorn, D., Rijs, K., Limpens, R. W. A. L., Groen, K., Koster, A. J., Snijder, E. J., Kikkert, M., & Bárcena, M. (2017). Expression and cleavage of middle east respiratory syndrome coronavirus nsp3-4 polyprotein induce the formation of double-membrane vesicles that mimic those associated with coronaviral rna replication. *MBio*, *8*(6), e01658-17. https://doi.org/10.1128/mBio.01658-17

Piña, F. J., Fleming, T., Pogliano, K., & Niwa, M. (2016). Reticulons regulate the er inheritance block during er stress. *Developmental Cell*, *37*(3), 279–288. https://doi.org/10.1016/j.devcel.2016.03.025

Piña, F., Yagisawa, F., Obara, K., Gregerson, J. D., Kihara, A., & Niwa, M. (2018). Sphingolipids activate the endoplasmic reticulum stress surveillance pathway. *Journal of Cell Biology*, *217*(2), 495–505. https://doi.org/10.1083/jcb.201708068

Preuss, D., Mulholland, J., Kaiser, C. A., Orlean, P., Albright, C., Rose, M. D., Robbins, P. W., & Botstein, D. (1991). Structure of the yeast endoplasmic reticulum: Localization of ER proteins using immunofluorescence and immunoelectron microscopy. *Yeast*, *7*(9), 891–911. https://doi.org/10.1002/yea.320070902

Raiborg, C., & Stenmark, H. (2009). The ESCRT machinery in endosomal sorting of ubiquitylated membrane proteins. *Nature*, *458*(7237), 445–452. https://doi.org/10.1038/nature07961

Ron, D., & Walter, P. (2007). Signal integration in the endoplasmic reticulum unfolded protein response. *Nature Reviews Molecular Cell Biology*, *8*(7), 519–529. https://doi.org/10.1038/nrm2199

Sakai, Y., Kawachi, K., Terada, Y., Omori, H., Matsuura, Y., & Kamitani, W. (2017). Two-amino acids change in the Nsp4 of SARS coronavirus abolishes viral replication. *Virology*, *510*, 165–174. https://doi.org/10.1016/j.virol.2017.07.019

Schwarz, D. S., & Blower, M. D. (2016). The endoplasmic reticulum: Structure, function and response to cellular signaling. *Cellular and Molecular Life Sciences*, *73*(1), 79–94. https://doi.org/10.1007/s00018-015-2052-6

Shulla, A., & Randall, G. (2016). (+) RNA virus replication compartments: A safe home for (Most) viral replication. *Current Opinion in Microbiology*, *32*, 82–88. https://doi.org/10.1016/j.mib.2016.05.003

Sicari, D., Chatziioannou, A., Koutsandreas, T., Sitia, R., & Chevet, E. (2020). Role of the early secretory pathway in SARS-CoV-2 infection. *Journal of Cell Biology*, *219*(9), e202006005. https://doi.org/10.1083/jcb.202006005

Snijder, E. J., Limpens, R. W. A. L., de Wilde, A. H., de Jong, A. W. M., Zevenhoven-Dobbe, J. C., Maier, H. J., Faas, F. F. G. A., Koster, A. J., & Bárcena, M. (2020). A unifying structural and functional model of the coronavirus replication organelle: Tracking down RNA synthesis. *PLOS Biology*, *18*(6), e3000715. https://doi.org/10.1371/journal.pbio.3000715

Voeltz, G. K., Rolls, M. M., & Rapoport, T. A. (2002). Structural organization of the endoplasmic reticulum. *EMBO Reports*, *3*(10), 944–950. https://doi.org/10.1093/embo-reports/kvf202

von Appen, A., LaJoie, D., Johnson, I. E., Trnka, M. J., Pick, S. M., Burlingame, A. L., Ullman, K. S., & Frost, A. (2020). LEM2 phase separation promotes ESCRT-mediated nuclear envelope reformation. *Nature*, *582*(7810), 115–118. https://doi.org/10.1038/s41586-020-2232-x

Webster, B. M., Colombi, P., Jäger, J., & Lusk, C. P. (2014). Surveillance of nuclear pore complex assembly by escrt-iii/vps4. *Cell*, *159*(2), 388–401. https://doi.org/10.1016/j.cell.2014.09.012

Westrate, L. M., Lee, J. E., Prinz, W. A., & Voeltz, G. K. (2015). Form follows function: The importance of endoplasmic reticulum shape. *Annual Review of Biochemistry*, *84*(1), 791–811. https://doi.org/10.1146/annurev-biochem-072711-163501

Wolff, G., Limpens, R. W. A. L., Zevenhoven-Dobbe, J. C., Laugks, U., Zheng, S., de Jong, A. W. M., Koning, R. I., Agard, D. A., Grünewald, K., Koster, A. J., Snijder, E. J., & Bárcena, M. (2020). A molecular pore spans the double membrane of the coronavirus replication organelle. *Science*, *369*(6509), 1395–1398. https://doi.org/10.1126/science.abd3629

Wright, R., Basson, M., D'Ari, L., & Rine, J. (1988). Increased amounts of HMG-CoA reductase induce "karmellae": A proliferation of stacked membrane pairs surrounding the yeast nucleus. *Journal of Cell Biology*, *107*(1), 101–114. https://doi.org/10.1083/jcb.107.1.101

Yang, H.-J., Asakawa, H., Haraguchi, T., & Hiraoka, Y. (2015). Nup132 modulates meiotic spindle attachment in fission yeast by regulating kinetochore assembly. *Journal of Cell Biology*, *211*(2), 295–308. https://doi.org/10.1083/jcb.201501035